ELSEVIER

Signal Processing 46 (1995) 345–362

SIGNAL PROCESSING

A multiscale vision model adapted to tne astronomical images

Albert Bijaoui*, Frédéric Rué

Observatoire de la Côte d'Azur, Dpt CERGA URA CNRS 1360, B.P. 229, 06304 Nice, Cedex 4, France

Received 1 September 1994; revised 10 January 1995 and 23 June 1995

Abstract

The analysis of the sky shows many kinds of hierarchically distributed objects. We have introduced a multiscale vision model based on the wavelet transform. The discrete transform is performed by the *à trous* algorithm which furnishes an isotropic vision, with a unique wavelet function. The vision model is based on the notion of the significant structures. We identify the pixels of the wavelet transform space (WTS) we can attribute to the objects. At each scale a region labelling is done. An interscale connectivity graph is then established. Connected trees are identified from the preceding graph. An object is generally associated to a subtree built from this graph. The identification of WTS pixels related to a given object leads to reconstructing an image by partial restoration algorithms. The object properties are extracted from the restored image. The main difficulty lies in the object reconstruction knowing the wavelet coefficients in the volume where the object is defined. It is a classical inverse problem. We choose to solve it using iterative algorithms. These algorithms give correct restored images, as we show on different examples, without or with adding a Gaussian noise. The influence of close objects can be partially removed.

Zusammenfassung

Die Analyse des Himmels zeigt viele Arten hierarchisch angeordneter Objekte. Wir haben ein Polyskalen-Modell für das Sehen auf der Grundlage der Wavelet-Transformation eingeführt. Die diskrete Transformation wird durch den *à trous*-Algorithmus durchgeführt, welcher eine isotrope Ansicht liefert, mit einer eindeutigen Waveletfunktion. Das Modell für das Sehen beruht auf der Angabe der kennzeichnenden Strukturen. Wir identifizieren die Pixel im Wavelet-transformationsraum (WTS), die wir den Objekten zuordnen können. Bei allen Skalenwerten werden die Regionen markiert. Dann wird ein Interskalen-Zusammenhangsgraph aufgebaut. Verbundene Bäume werden vom vorangegangenen Graphen her identifiziert. Im allgemeinen wird ein Objekt mit einem Teilbaum in Verbindung gebracht, der aus diesem Graph gebildet wird. Die Identifikation von WTS-Pixeln, die mit einem bestimmten Objekt zu tun haben, führt auf die Rekonstruktion eines Bildes durch Teil-Restaurationsalgorithmen. Die Objekteigenschaften werden aus dem restaurierten Bild extrahiert. Die Hauptschwierigkeit liegt in der Objektrekonstruktion, wenn die Waveletkoeffizienten in dem räumlichen Gebiet bekannt sind, in dem das Objekt definiert ist. Es handelt sich um ein klassisches inverses Problem. Wir wählen iterative Verfahren zu ihrer Lösung. Diese Algorithmen liefern korrekt restaurierte Bilder, wie wir anhand verschiedener Beispiele zeigen, ob nun ein gaußsches Störrauschen addiert wird oder nicht. Der Einfluß dicht benachbarter Objekte kann teilweise beseitigt werden.

* Corresponding author. E-mail: bijaoui@obs-nice.fr.

SSDI 0165-1684(95)00093-3

Résumé

L'observation du ciel met en évidence de nombreux types d'objets distribués hiérarchiquement. Nous avons introduit un modèle de vision multi-échelles basé sur la transformation en ondelettes. La transformation discrète est réalisée par l'algorithme *à trous*, lequel permet une vision isotrope, avec une seule fonction ondelette. Le modèle de vision est fondé sur la notion de structures significatives. Lex pixels de l'espace de la transformation en ondelettes (WTS), pouvant être attribués aux objets, sont identifiés. A chaque échelle, une procédure de segmentation est appliquée. Un graphe d'inclusion des domaines d'une échelle à l'autre est alors établi, A partir de ce graphe, on identifie des arbres connexes. A chaque sous-arbre du graphe d'inclusion, est associé généralement un objet. L'identification des pixels du WTS attribués à un objet donné, conduit à reconstruire une image, grâce à des algorithmes de restauration partielle. A partir de ces images, on peut alors extraire les propriétés des objets. La principale difficulté réside dans la reconstruction de l'image d'un objet connaissant le volume de coefficients en ondelettes où il est défini. C'est un problème inverse classique. Nous avons choisi de le résoudre en appliquant des algorithmes itératifs. Ces algorithmes donnent des images restaurées de bonne qualité, tout à fait utilisables, comme le montrent différents exemples avec ou sans bruit additif gaussien. L'influence des objets proches peut être partiellement supprimée.

Keywords: Multiscale vision; Wavelet transform; Image processing; Image restoration

1. Artificial vision and astronomical images

The astronomical images contain typically a large set of point-like sources (the stars), some quasi-point-like objects (faint galaxies, double stars, etc.) and some complex and diffused structures (galaxies, nebulous, planetary stars, clusters, etc.). A *vision model* is defined by the sequence of operations required for the automated image analysis. Astronomical images need specific ones which take into account the scientific purposes, the characteristic of the objects and the existence of hierarchial structures.

The classical vision model for robotic and industrial images is based on the detection of the edges. We have applied first this conception to the astronomical imagery [4]. We choose the Laplacian of the intensity as the edge line. The results are independent of large-scale spatial variations, such as the ones due to the sky background. The main disadvantage of the resulting model lies in the difficulty to get a correct object classification: astronomical sources cannot be accurately recognized from their edges.

Many reduction procedures were built using a model for which the image is the sum of a slowly variable background with superimposed small-scale objects [24, 22]. We build first a background mapping [2]. For that purpose we need to introduce a scale: the background is defined in a given area. Each pixel with a value significantly greater than the background is considered to belong to a real object. The same label is given to each significant pixel belonging to the same connected field. For each field we determine the area, the position, the flux and some pattern parameters. Generally, this procedure leads to quite accurate measurements, with a correct detection and recognition. The model works very well for poor fields. If this is not the case, a labelled field may correspond to many objects. The background map is done at a given scale: larger objects are removed. The smoothing is only adapted to the star detection, not to larger objects.

An improvement of the previous model is done with the introduction of the *radial profile* of each source [13, 21]. An astronomical object is associated to a point-like structure. We have thus only to detect the local maxima. The radial profile contains the main information on the source structure. Compared to the previous models, the quality of the measurements is increased, and the derived pattern parameters allow a gain in the separation between the stars and the galaxies. This procedure does not allow to describe complex structures. The method is adapted to quasi-stellar sources, on a slowly varying background.

In fact, the three vision models we used on many sets of images failed to bring a complete analysis because they are based on a single spatial scale for

the adapted smoothing and for the background mapping. A multiscale analysis allows to get a background adapted to a given object and to optimize the detection of different size objects. We expected that the wavelet transform was the tool allowing us to build an analysis taking into account all the constraints.

2. The multiscale approach

2.1. The continuous wavelet transform

Morlet–Grossmann's [16] definition for a 1D function $f(x) \in L^2(R)$ is

$$w(a, b) = \frac{1}{\sqrt{a}} \int_{-\infty}^{+\infty} f(x) \psi^* \left(\frac{x - b}{a} \right) \mathrm{d}x, \tag{1}$$

$\psi(x)^*$ designs the conjugate of the analyzing wavelet $\psi(x)$, a (> 0) the scale parameter and b the position parameter. The wavelet transform is a linear transformation, covariant under translations and dilations.

Consider now a function $w(a, b)$ which is the wavelet transform of a given function $f(x)$. It was shown [9] that $f(x)$ can be restored with the formula

$$f(x) = \frac{1}{C_\psi} \int_0^{+\infty} \int_{-\infty}^{+\infty} \frac{1}{\sqrt{a}} w(a, b) \psi \left(\frac{x - b}{a} \right) \frac{\mathrm{d}a \, \mathrm{d}b}{a^2}, \tag{2}$$

with

$$C_\psi = \int_0^{+\infty} \frac{|\hat{\psi}(\nu)|^2}{\nu} \mathrm{d}\nu, \tag{3}$$

where $\hat{\psi}(\nu)$ designs the Fourier transform of $\psi(x)$. The reconstruction is only correct if C_ψ is defined (admissibility condition). This is generally true if $\hat{\psi}(0) = 0$, i.e. the mean of the wavelet function is 0.

Many 2D extensions of the continuous wavelet transform are possible: from identical dilations on coordinates, using an isotropic wavelet function, from dilations independently for each axis, from identical dilations, with rotations of the wavelet pattern in Fourier space, using an anisotropic wavelet function [17], from independent dilations and rotations. The dimension of the resulting transform depends on the choice: 3 for the first one, 4 for the two following ones, and 5 for the last one. This is one of the reasons which led us to choose an isotropic wavelet. Another reason lies in the physical data interpretation, an isotropic wavelet transform provides an isotropic vision and easily understandable parameters.

2.2. The discrete wavelet transform from the multiresolution analysis

The use of the wavelet transform with a computer can be foreseen through the sampling theorem [5]. The wavelet transform is a set of convolutions, so if we process an image with a cutoff frequency, we just have to do some multiplications in the Fourier space. The number of elements for a scale can be reduced if the frequency bandwidth is also reduced. This is correct only for wavelets having also a cutoff frequency. Littlewood–Paley's decomposition [14], based on an iterative dichotomy of the frequency band, provides a very nice illustration of the reduction of elements scale by scale.

The *multiresolution analysis* [15] is an extension of Littlewood–Paley's decomposition to a large class of wavelets. It is based on an increasing sequence of closed linear subspace V_i of $L^2(R)$, where i is an integer. A function $f(x)$ is projected at each step i on the subset V_i. This projection is defined by the scalar product $c(i, k)$ of $f(x)$ with the function $\phi(x)$ which is dilated and translated:

$$c(i, k) = \frac{1}{2^i} \left\langle f(x), \phi \left(\frac{x}{2^i} - k \right) \right\rangle, \tag{4}$$

$\phi(x)$ is named the scaling function of the analysis. Its main property lies in the following relation (dilation equation [25]):

$$\frac{1}{2} \phi \left(\frac{x}{2} \right) = \sum_{n=n_1}^{n_2} h(n) \phi(x - n). \tag{5}$$

This relation allows to compute the set $\{c(i, k)\}$ from $\{c(i - 1, k)\}$:

$$c(i, k) = \sum_{n=n_1}^{n_2} h(n - 2k) c(i - 1, n). \tag{6}$$

The coefficients $c(i, k)$ are obtained iteratively by convolution with the low-pass filter $h(-n)$, followed by a decimation. For some scaling functions n_1 and n_2 are limited, and we have a classical FIR filtering. At each step, the number of scalar products are divided by 2. Some information is lost, and step by step the signal is smoothed. The remaining information can be restored using the complementary subspace W_i of V_i in V_{i-1}. This subspace can be generated by a suitable wavelet function $\psi(x)$ with translation and dilation. We have

$$\frac{1}{2}\psi\left(\frac{x}{2}\right) = \sum_{n=n_3}^{n_4} g(n)\phi(x-n). \tag{7}$$

We compute the scalar products $(1/2^i)\langle f(x), \psi(x/2^i - k)\rangle$, i.e. the discrete wavelet coefficients, with

$$w(i, k) = \sum_{n=n_3}^{n_4} g(n-2k)c(i-1, n). \tag{8}$$

The coefficients $w(i, k)$ are obtained by convolution with the high-pass filter $g(-n)$, followed by a decimation. If n_3 and n_4 are limited, we have another FIR filtering. In the case of orthogonal wavelets the filters $h(n)$ and $g(n)$ are conjugated [15] and we have the relation

$$g(n) = (-1)^{1-n}h(1-n). \tag{9}$$

The 2D multiresolution analysis is generally performed separately in line and column. This does not lead to an isotropic vision, three wavelet functions are used and it is not easy to associate wavelet coefficients to a given pixel. Stars, and more generally astronomical sources, are quite isotropic sources, no direction is privileged Thus we choose an isotropic wavelet transform. We need also to do a connection between images at different scales. As the redundancy is not critical we prefer to avoid the decimation. This led us to use the *à trous* algorithm [11, 3].

2.3. The à trous algorithm

Let us consider the 1D algorithm. As for the multiresolution analysis, we admit that the sampled data are the scalar product of the function with translated scaling functions:

$$c(0, k) = \langle f(x), \phi(x-k)\rangle. \tag{10}$$

Let us consider the scalar products at the scale i:

$$c(i, k) = \frac{1}{2^i}\left\langle f(x), \phi\left(\frac{x-k}{2^i}\right)\right\rangle. \tag{11}$$

If $\phi(x)$ satisfies the dilation equation, we compute easily $c(i, k)$ from a scale to the double one from the relation

$$c(i, k) = \sum_n c(i-1, k+2^{i-1}n)h(n). \tag{12}$$

The wavelet coefficient at scale 2^i and at location k is computed from

$$w(i, k) = \sum_n c(i-1, k+2^{i-1}n)g(n). \tag{13}$$

We have no decimation, i.e. no factor 2 before k. Therefore we need a larger step between the points. The jump of $2^{i-1}-1$ pixels in the convolutions gives its name to this algorithm. The choice of the filter $h(n)$ is not arbitrary. Generally the solution of the dilation equation is irregular, and it cannot be used for the algorithm [6]. B-spline interpolations [26] are generated by binomial coefficients. For example, $B_3(x)$ leads to the set $\{\frac{1}{16}; \frac{1}{4}; \frac{3}{8}; \frac{1}{4}; \frac{1}{16}\}$ $(-2 \leqslant n \leqslant 2)$. It is the choice we do in our procedure.

For the choice of the filter $g(n)$ we use the wavelet resulting from the difference between two successive interpolations:

$$w(i, k) = c(i, k) - c(i-1, k). \tag{14}$$

So we get an easy reconstruction algorithm by adding all the wavelet images with the smoothest one.

The 2D algorithm works with a product of B-splines for the successive interpolations. $B_3(x)$ is close to a Gaussian function and the results are quasi-isotropic. With $B_5(x)$ the discrepancy to the Gaussian is very small, and the interpolation and the wavelet can be considered as isotropic.

2.4. Application to an astronomical image

Fig. 1 shows the image of the galaxy NGC2997. In Fig. 2 we have plotted the image of the wavelet

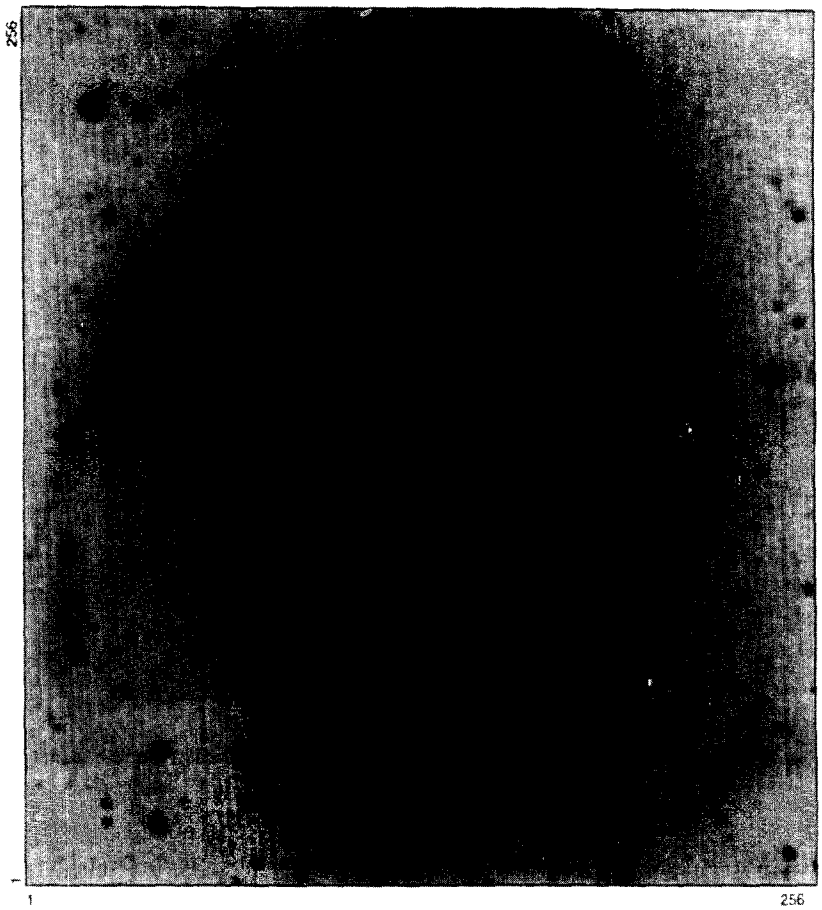

Fig. 1. Image of the galaxy NGC2997.

transform for three scales, and for the smoothed image at the fourth scale. If we add these four images we get exactly the original image.

The wavelet images correspond to different spatial frequency bands. They show structures of different size; in the first image we see only the noise and some stars, while in the third one we can observe great structures like the galaxy arms.

In Fig. 3, the wavelet transform is plotted with isolevel lines. For each scale we determine the standard deviation σ_i of the distribution of the wavelet coefficients. Then we plotted the isolevel lines corresponding to the values $3\sigma_i$. This visualization is more compact than the previous one and shows the connections between the structures at different scales.

3. The object definition in the wavelet transform space

3.1. The basis of the object definition

After applying the wavelet transform on the image, we have to detect, extract, measure and recognize the significant structures. The wavelet space is a 3D one. An object has to be defined in this space. A general idea for the object definition lies in the connectivity property. An object occupies a physical region, and in this region we can join any pixel to other ones. The connectivity in the direct space has to be transported to the wavelet transform space (WTS). In order to define the objects we have to identify the WTS pixels we can attribute to the objects.

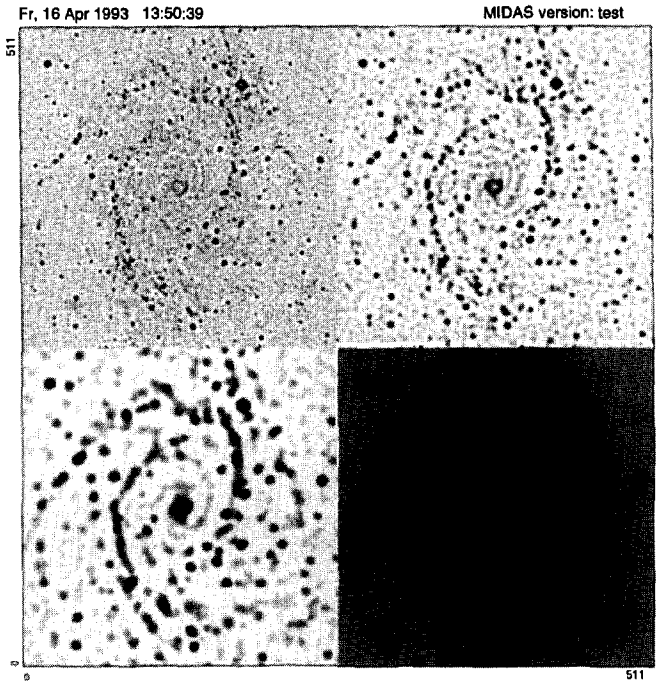

Fig. 2. Wavelet transform of the galaxy. Three wavelet scales and the last smoothed image.

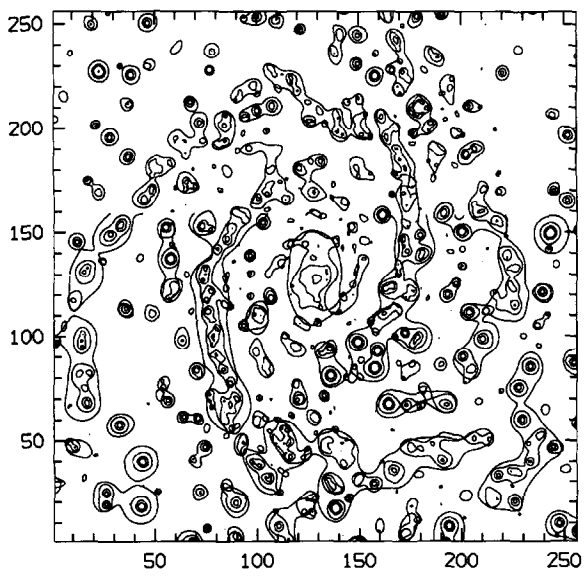

Fig. 3. Isolevels of the wavelet transform of galaxy NGC2997 for three scales.

At a given scale, it is clear that a given object leads to one connected field. A region labelling has to be done, scale by scale. A physical object can show features at different successive scales, an inter-scale connectivity graph has then to be established. Connected trees are identified from the preceding graph, they correspond to a WTS region which can be associated to a complex object. An object is more generally associated at a subtree. This permits to separate close components and to identify an object from its full components. The identification of WTS pixels related to a given object leads to reconstruct an image by partial restoration algorithms.

3.2. The thresholding in the wavelet space

3.2.1. The statistical distribution of the wavelet coefficients

The statistical distribution of the wavelet coefficient depends on the noise process. In this paper,

we admit that we have a stationary Gaussian white noise for the image. In the case of a Poissonian noise, we can transform the pixel intensity by Anscombe's transform [1] and process the data as Gaussian variables. This transform gives correct results for photon counts greater than about 30 per pixel, which is generally the case. For CCD observations, the noise is described by the sum of a Gaussian and a Poissonian variable, and we have generalized Anscombe's transform, which leads also to a Gaussian variable [18]. For a simple presentation of our vision model we further admit that the noise is Gaussian.

We could analytically examine the noise distribution of the wavelet coefficients, but we have proceeded by simulation. We compute the image of a simulated Gaussian noise with a variance 1 and no correlation from a pixel to its neighbors. Then we compute its discrete wavelet transform and we estimate the standard deviation $\sigma_n(i)$ at each scale. For the image to be processed, the standard deviation $\sigma(1)$ is estimated from the histogram of the wavelet coefficients $w(1, k, l)$. At this scale, the wavelet coefficient values essentially result from the noise. Knowing the variation of the noise with the scale from the simulation we deduce the $\sigma(i)$ set.

3.2.2. The significant pixels

After the determination at each scale of the distribution of the wavelet coefficients $w(i, k, l)$ taking into account the noise, we can introduce a statistical meaning of its value from the classical decision theory [10]. $\mathscr{H}_0$ is the hypothesis that at the scale i the image is constant in the neighborhood of the pixel (k, l). The $w(i, k, l)$ distribution is a Gaussian of mean 0 of standard deviation $\sigma(i)$. Its probability distribution is

$$p(w(i, k, l)) = \frac{1}{\sqrt{2\pi}\,\sigma(i)} \exp\left[\frac{w^2(i, k, l)}{2\sigma^2(i)}\right]. \tag{15}$$

For a positive coefficient, the $\mathscr{H}_0$ rejection depends on the probability:

$$P = \text{Prob}(W > w(i, k, l))$$

$$= \frac{1}{\sqrt{2\pi}\,\sigma(i)} \int_{w(i,k,l)}^{+\infty} \exp\left[-\frac{W^2}{2\sigma^2(i)}\right] dW. \tag{16}$$

For a negative coefficient we examine

$$P = \text{Prob}(W < w(i, k, l))$$

$$= \frac{1}{\sqrt{2\pi}\,\sigma(i)} \int_{-\infty}^{w(i,k,l)} \exp\left[-\frac{W^2}{2\sigma^2(i)}\right] dW. \tag{17}$$

We fix a decision level ε. If $P > \varepsilon$, $\mathscr{H}_0$ is not excluded, and the coefficient value can be due to the noise. On the contrary, if $P < \varepsilon$, we cannot consider at this decision level that the value results only from the noise and $\mathscr{H}_0$ must be rejected. We say that we have detected a significant coefficient.

This vision model is based only on the detected significant pixels. Taking into account the noise properties, we have only to compare $w(i, k, l)$ to $k\sigma(i)$, where k is a function of ε. We generally choose $k = 3$.

3.3. The scale by scale field labelling

After the identification of the significant pixels we do an image segmentation scale/scale in WTS. In our present analysis we have examined only positive coefficients, which correspond to light sources. Significant negative pixels may be associated to absorbing regions, but they are generally associated to the wavelet bumps: around a peak we have always negative wavelet coefficients. The corresponding pixels do not belong to a real object, even if they are significant.

The region labelling is done by a classical growing technique. At each scale, we give a label to a pixel: 0 if the wavelet coefficient is smaller than the threshold, $n > 0$ for the contrary case. Each close significant pixel has the same label. We design by $L(i, k, l)$ the label corresponding to the pixel (k, l) at the scale i.

An object could be defined from each labelled field without taking into account the interscale neighborhood. We can restore an image of these objects from the known wavelet coefficients, but this restoration would not use all the information. A given physical object may lead to significant pixels at different scale, a correct restoration needs the whole information.

3.4. The interscale relation

An astrophysical object is described as a hierarchical set of structures. So we have to link the labelled fields from a scale to the following one, in order to give the hierarchy.

Let us consider a field A at a scale i and a field B with a label b at scale $i+1$. (k_a, l_a) corresponds to the pixel coordinates of the maximum coefficient $w(i, k_a, l_a)$ of A. We say that A is connected to B if

$$L(i+1, k_a, l_a) = b. \tag{18}$$

The maximum position belongs at scale $i+1$ to the field B.

3.5. The interscale connection trees

From the preceding steps we have obtained a set of fields $D(i, n)$ and a relation $\mathcal{I}$:

$$D(i, n)\mathcal{I}D(i+1, m) \quad \text{if } L(i+1, k_n, l_n) = m, \tag{19}$$

where (k_n, l_n) are the pixel coordinates of the maximum value in the field $D(i, n)$.

This relation leads to building a set of (directed-) trees $\mathcal{T}_l$. The trees result from the field inclusions from the largest scale to the smallest one. After this operation we can say if a large scale field contains smaller ones which contain smaller ones, and so on.

An element of a given tree $\mathcal{T}_l$ is a field $D(i, n)$. Two fields $D(i, n)$ and $D(j, m)$ belong to the same tree if there exists a field $D(k, p)$ such that

$$D(i, n)\mathcal{I}D(i+1, n_1)\cdots\mathcal{I}D(k, p), \tag{20}$$

$$D(j, m)\mathcal{I}D(j+1, m_1)\cdots\mathcal{I}D(k, p). \tag{21}$$

All the fields belonging to the same tree $\mathcal{T}_l$ have the same ancestor, the root, $D(k_l, p_l)$ where k_l is the largest scale for this tree and p_l the corresponding field of pixels.

The tree can be easily constructed from its root by identifying from the largest scale to the smallest ones the fields which are connected. The leaves are the fields which are not connected to smallest-scale ones. Evidently a given field $D(i, n)$ belongs to only one tree.

3.6. An object as a subtree

From the image we can extract a set of connected trees, corresponding to different objects. We could define an object as one tree, but it appears that we reduce in a too high manner the number of objects. A small star may belong to a small nebula, the tree corresponds to the nebula, and we do not consider the star if we take into account only the connected tree. It is the reason why we define an object as a subtree resulting from the image segmentation in the wavelet space. The considered subtrees are only the ones generated by all the fields which have a given field $D(k, p)$ as ancestor. A subtree contains necessarily the leaves.

We consider a field $D(i+1, m)$ which is connected to two fields $D(i, n_1)$ and $D(i, n_2)$. From these two fields we can construct the two subtrees $\mathcal{S}_1$ and $\mathcal{S}_2$. Each subtree corresponds to a WTS region. We will examine in the next section how we can reconstruct the image of each object associated to each region. They are two different components of the image.

From $D(i+1, m)$ we built another subtree $\mathcal{S}$ which contains $\mathcal{S}_1$, $\mathcal{S}_2$ and $D(i+1, m)$. In WTS we have merged the two regions and connected them by a bridge formed by the $D(i+1, m)$ pixels. In this space, the new extracted region is connected too. We reconstruct the image of an object which not only contains the previous components, but also takes into account an original information at scale $i+1$. It really corresponds to a new object.

3.7. The identification of the objects

We can summarize now this method allowing to identify all the objects in a given image:

1. We compute the wavelet transform with the *à trous* algorithm, which leads to a set $w(i, k, l)$, $i \leqslant I$.
2. We determine the standard deviation of $w(1, k, l)$ due to the noise.
3. We deduce the thresholds at all the scales.
4. We threshold scale by scale and we do an image labelling.
5. We determine the interscale relations.
6. We extract all the connected trees from the interscale relations.

7. We identify all the subtrees following our definition.

Let us remark that this definition is very sensitive to the kind of wavelet transform done. We work with an isotropic wavelet, without decimation. With Mallat's algorithm this definition must be revised.

4. The partial reconstruction

4.1. The basic problem

Let us consider now an object $\mathcal{O}$ previously defined. It corresponds to a volume $\mathcal{D}$ in WTS. This volume is associated to a set $\mathcal{V}$ of wavelet coefficients such that

$$\mathcal{O} \Rightarrow \{\mathcal{V}(i,k,l), \text{ for } (i,k,l)\in\mathcal{D}\}. \tag{22}$$

$\mathcal{F}$ is an image and $\mathcal{W}$ is its corresponding wavelet transform. $\mathcal{F}$ can be considered as a correct restored image of the object $\mathcal{O}$ if

$$\mathcal{V}(i,k,l) = \mathcal{W}(i,k,l) \quad \forall (i,k,l)\in\mathcal{D}. \tag{23}$$

$P_{\mathcal{D}}$ designs the projection operator in the subspace $\mathcal{D}$ and WT the operator associated to the wavelet transform; we can write

$$\mathcal{V} = (P_{\mathcal{D}} \circ WT)\mathcal{F} = \mathcal{M}\mathcal{F}. \tag{24}$$

We have to solve the inverse problem which consists of determining $\mathcal{F}$ knowing $\mathcal{M}$ and $\mathcal{V}$. The solution of this problem depends on the regularity of $\mathcal{M}$. In many papers and books authors have discussed the availability of a solution to this class of inverse problems (for example see [7]). The size KL of the restored image is arbitrary and it can be easily set greater than the number of known coefficients. It is sure that there exists an image $\mathcal{F}$ which gives exactly $\mathcal{V}$ in $\mathcal{D}$, the original one: the equation is consistent [19]. But generally we have an infinity of solutions, and we have to choose among them the one which is considered as the correct one. The image is always a positive function, which leads to constrain the solution, but this is not sufficient to get a single one.

The choice is governed by a regularization condition. Many regularization conditions were developed for the restoration. Taking into account the consistency, we used first a direct simple algorithm, connected to Van Cittert's one [27] for which the regularization is done by the limitation of the support. Then we applied another iterative algorithm which corresponds to minimizing the energy.

4.2. Restoration by the direct algorithm

Eq. (23) seems trivial but $\mathcal{W}(i,k,l)$ has to be known for all coefficients, while $\mathcal{V}(i,k,l)$ is known only in $\mathcal{D}$. The problem is to build an array $\mathcal{W}(i,k,l)$ solution of the equation, but which corresponds to the discrete wavelet transform of a positive discrete image.

The wavelet transform $W = W(i,k,l)$ is conventionally split into two arrays W_{in} and W_{out} so that $W = W_{\text{in}} + W_{\text{out}}$, with

$$W_{\text{in}} = \begin{cases} W(i,k,l) & \text{if } (i,k,l)\in\mathcal{D}, \\ 0 & \text{if } (i,k,l)\notin\mathcal{D} \end{cases} \tag{25}$$

and

$$W_{\text{out}} = \begin{cases} 0 & \text{if } (i,k,l)\in\mathcal{D}, \\ W(i,k,l) & \text{if } (i,k,l)\notin\mathcal{D}. \end{cases} \tag{26}$$

These definitions are useful in the following developments but W_{in} and W_{out} cannot be considered as the wavelet transform of given images, they are only *wavelet structures*.

The direct algorithm takes into account the fact that we have not to modify the values of the wavelet transform inside $\mathcal{D}$, but only outside. From this remark we get the relations

$$\begin{aligned} \mathcal{W}_{\text{in}}^{(n)} &= \mathcal{V}_{\text{in}}, \\ \mathcal{W}_{\text{out}}^{(n)} &= V_{\text{out}}^{(n-1)}, \end{aligned} \tag{27}$$

where $V^{(n)}(i,k,l)$ is the wavelet transform of the image reconstructed from $\mathcal{W}^{(n)}(i,k,l)$. On account of the redundancy of the *à trous* algorithm, $V^{(n)}(i,k,l)$ is not equal to $\mathcal{W}^{(n)}(i,k,l)$.

In order to test the validity of the algorithms we considered first a Gaussian pattern rather typical of the image of an astronomical object. We start without any noise in order to examine the quality of the inversion. In Fig. 4 we plotted the isolevels of the considered Gaussian pattern. We do a set of

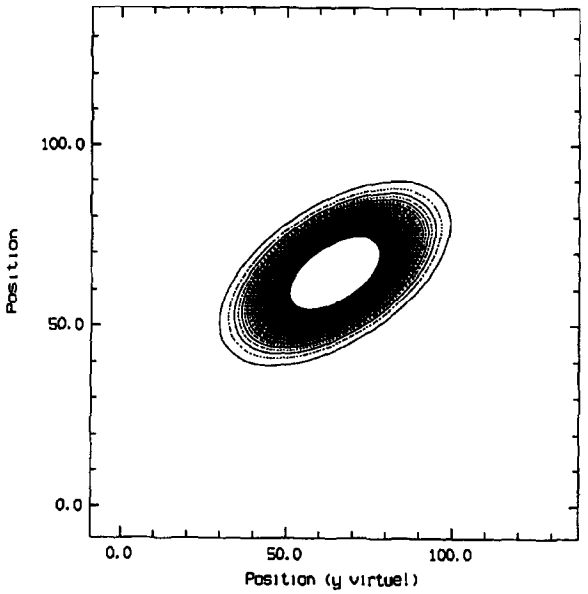

Fig. 4. Gaussian pattern without noise.

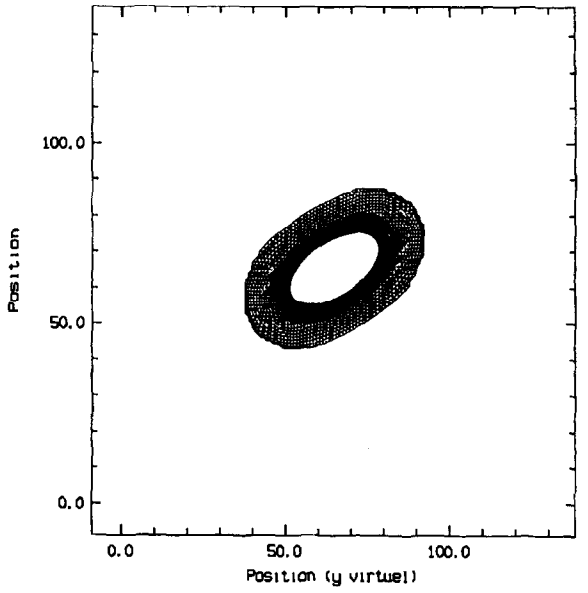

Fig. 5. Restoration Gaussian pattern without noise by the direct algorithm.

numerical experimentations but this elongated pattern is well adapted to show the quality of the restoration.

We keep only the positive coefficients; in Fig. 5 we show the restored image with the direct algorithm. After a few iterations (4–5) the image is quite stabilized, the residue between $\mathscr{W}_{in}$ and $\mathscr{V}_{in}$ is very small, but there exists a discrepancy between the resulting Gaussian parameters and the original ones. After about 30 iterations the convergence is correct.

The object corresponds to a subtree $\mathscr{T}$. At the largest scale, the maximum of the wavelet coefficient is $W(i_t, k_t, l_t)$. We need for a rapid convergence that

$$W(i_t, k_t, l_t) > W(i_t + 1, k_t, l_t). \tag{28}$$

If this condition is not respected, the discrepancy between the restored and the original Gaussian parameters can be very important for a few iterations, and the convergence is not assured. The algorithm restores an image but a part of the information is lost.

The restored image $\mathscr{F}$ is compact: outside a field $\mathscr{S}$ the values of $\mathscr{F}$ are null. The support compactness results from the thresholding of negative values. In Fig. 6 we have plotted the support of the function $\mathscr{F}(k, l)$ in the case of the Gaussian pattern. The support is stable from the first iteration.

This reconstitution algorithm allows to restore quite exactly a Gaussian pattern knowing the wavelet coefficients in a compact region of the WTS. The accuracy is increasing with the number of considered scales, but a minimum of scales is necessary.

4.3. Restoration by using the gradient

The gradient is naturally introduced when we want to minimize the distance $\|Y - A(X)\|$ between Y and the convolved solution $A(X)$. We get the iterative relation [12]

$$X^{(n)} = X^{(n-1)} + \omega\tilde{A}(Y - A(X^{(n-1)})). \tag{29}$$

$\tilde{A}$ is the joint operator associated to A and ω is a scalar to be estimated. We obtain with our previous notations

$$\mathscr{F}^{(n)} = \mathscr{F}^{(n-1)} + \omega\tilde{\mathscr{M}}(\mathscr{V} - \mathscr{M}(\mathscr{F}^{(n-1)})). \tag{30}$$

The main difficulty lies in the understanding of the joint operator $\tilde{\mathscr{M}}$ which transforms a wavelet transform into an image.

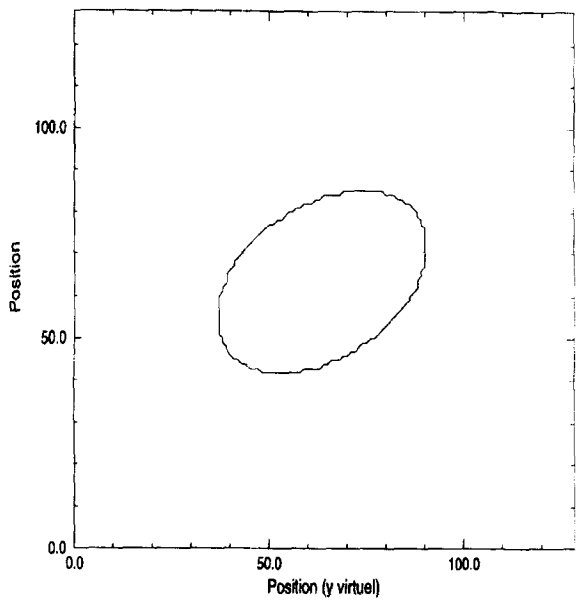

Fig. 6. Support of the function resulting from the direct algorithm for the Gaussian pattern. This support is stable from the first iteration.

Proposition. *If W is a wavelet structure and $\tilde{F}$ the resulting image of $\tilde{\mathscr{M}}(W)$, we have*

$$\tilde{F} = \tilde{\mathscr{M}}(W) = \sum_{i=1}^{I} \{WT[W(i,k,l)]\}_i, \tag{31}$$

where $\{WT[F(k,l)]\}_i$ is the discrete wavelet transform of the array $F(k,l)$ at the scale i.

From the *à trous* algorithm we get the wavelet and the smoothing coefficients:

$$W(i,k,l) = \sum_{n,m} g(n,m)F(i-1, k+2^{i-1}n, l+2^{i-1}m), \tag{32}$$

$$F(i,k,l) = \sum_{n,m} h(n)h(m)F(i-1, k+2^{i-1}n, l+2^{i-1}m).$$

We can find a discrete function $\gamma(i,k,l)$ so that

$$W(i,k,l) = \sum_{k',l'} \gamma(i, k-k', l-l')F(k',l') \tag{33}$$

if p is a pixel (i,k,l) in WTS; we can write

$$W(p) = \sum_{k',l'} m(p,k',l')F(k',l') \tag{34}$$

with

$$m(p,k',l') = \gamma(i, k-k', k-l'). \tag{35}$$

Now we restrict the relation only to $\mathscr{D}$:

$$\begin{aligned} W(p) &= \sum_{k',l'} m(p,k',l')F(k',l') \quad \text{for } p \in \mathscr{D}, \\ W(p) &= 0 \qquad\qquad\qquad\qquad \text{for } p \notin \mathscr{D}. \end{aligned} \tag{36}$$

We get now the result from the joint operator on $W(p)$:

$$\tilde{F}(k,l) = \sum_p m(p,k,l)W(p) \tag{37}$$

$$= \sum_{i,k',l'} \gamma(i, k'-k, l'-l)W(i,k',l') \tag{38}$$

$$= \sum_i \sum_{k',l'} \gamma(i, k'-k, l'-l)W(i,k',l'). \tag{39}$$

We note

$$\tilde{W}_i(j,k,l) = \sum_{k',l'} \gamma(j, k'-k, l'-l)W(i,k',l'). \tag{40}$$

$\tilde{W}_i(j,k,l)$ is the wavelet transform at scale j of the wavelet transform of the function $F(k,l)$ at scale i. We get finally

$$\tilde{F}(k,l) = \sum_i \tilde{W}_i(i,k,l). \tag{41}$$

4.3.1. The restoration algorithm

We have now the following steps:

1. Initialization: $\mathscr{F}^{(0)}$ is obtained from the reconstruction of $\mathscr{V}$.
2. Wavelet transform of the last approximation:
$$\tilde{V}^{(n-1)}(i,k,l) = WT[\mathscr{F}^{(n-1)}(k,l)]. \tag{42}$$
3. Projection of $\tilde{V}^{(n-1)}$ in $\mathscr{D}$:
$$V^{(n-1)}(i,k,l) = \tilde{V}^{(n-1)}(i,k,l) \quad \forall i \in \mathscr{D}, \tag{43}$$
$$V^{(n-1)}(i,k,l) = 0 \quad \text{if } i \notin \mathscr{D}. \tag{44}$$
4. Residual image obtained from the joint operator:
$$\begin{aligned} \mathscr{W}r^{(n-1)}(i,k,l) &= \mathscr{V}(i,k,l) - V^{(n-1)}(i,k,l), \\ \mathscr{F}r^{(n-1)}(k,l) &= \tilde{\mathscr{M}}(\mathscr{W}r^{(n-1)}) \\ &= \sum_{i=1}^{I} WT[(\mathscr{W}r^{(n-1)}(i,k',l')](i,k,l). \end{aligned} \tag{45}$$

5. Iterative correction:

$$\tilde{\mathscr{F}}^{(n)} = \mathscr{F}^{(n-1)} + \omega \mathscr{F} r^{(n-1)}. \tag{46}$$

6. Thresholding in order to get a positive function:

$$\mathscr{F}^{(n)} = \mathrm{Max}(0, \tilde{\mathscr{F}}^{(n)}). \tag{47}$$

7. Come back to step 2.

We test the $Wr^{(n)}(i, k, l)$ energy in order to stop the process.

4.3.2. Choice of ω

We note $q(X^{(n)}) = \| Y - A(X^{(n)}) \|$ and $\omega^{(n)}$ is ω at step n. We must have

$$q(X^{(n-1)}) < q(X^{(n)}). \tag{48}$$

We start from relation (29) written now:

$$X^{(n)} = X^{(n-1)} + \omega^{(n)} X r^{(n-1)}. \tag{49}$$

We have

$$q(X^{(n)}) = \| Y - A(X^{(n)}) \| \tag{50}$$

$$= \| Y - A(X^{(n-1)}) - \omega^{(n)} X r^{(n-1)} \| \tag{51}$$

$$= \| Y - A(X^{(n-1)}) \| + \omega^{(n)2} \| A(X r^{(n-1)}) \| - 2\omega^{(n)} \langle Y - A(X^{(n-1)}), A(X r^{(n-1)}) \rangle \tag{52}$$

$$= q(X^{(n-1)}) + \omega^{(n)2} \| A(X r^{(n-1)}) \| - 2\omega^{(n)} \langle \tilde{A}(Y - A(X^{(n-1)})), X r^{(n-1)} \rangle \tag{53}$$

$$= q(X^{(n-1)}) + \omega^{(n)2} \| A(X r^{(n-1)}) \| - 2\omega^{(n)} \| X r^{(n-1)} \|. \tag{54}$$

For $q(X^{(n-1)}) < q(X^{(n)})$ it is sufficient to have

$$\omega^{(n)} < \frac{2 \| X r^{(n-1)} \|}{\| A(X r^{(n-1)}) \|}. \tag{55}$$

$q(X^{(n)})$ is minimal for

$$\omega^{(n)} = \frac{\| X r^{(n-1)} \|}{\| A(X r^{(n-1)}) \|}. \tag{56}$$

In this case the convergence is optimal. Replacing $X r^{(n-1)}$ by $\mathscr{F} r^{(n-1)}$ we get

$$\omega^{(n)} < \frac{2 \| \mathscr{F} r^{(n-1)} \|}{\| \mathscr{M}(\mathscr{F} r^{(n-1)}) \|} = \frac{2 \| \mathscr{F} r^{(n-1)} \|}{\| \mathscr{W} r_{\mathrm{in}}^{(n-1)} \|}. \tag{57}$$

$\omega^{(n)}$ can be chosen constant (fix step or Landweber's algorithm) or adapted at each step (true gradient algorithm). As the energy is maintained in the wavelet transform, $\| \mathscr{F} r^{(n-1)} \|$ is always greater than $\| \mathscr{W} r_{\mathrm{in}}^{(n-1)} \|$. So we can choose for a fix step algorithm

$$\omega^{(n)} = \omega = 1. \tag{58}$$

4.3.3. Numerical experiment without noise

In Fig. 7 we show the restored image of the Gaussian pattern. Compared to the direct algorithm, the convergence is faster but the computing time is quite similar, taking into account the increase of the complexity for an iterative step. After about 20 iterations the convergence is correct. The number of needed scales is the same as previously.

The support of the restored image $\mathscr{F}$ is larger than the one resulting from the direct algorithm. In Fig. 8 we have plotted the evolution of the reconstruction support for a set of steps. Even if the image field is extended step by step, the support converges to a compact field. The quality of the restoration seems generally better after a few iterations. The profiles are smoother.

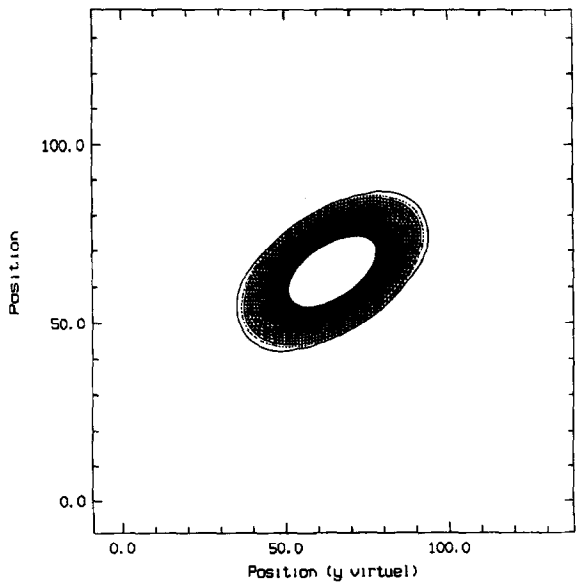

Fig. 7. Restoration Gaussian pattern without noise by the gradient algorithm.

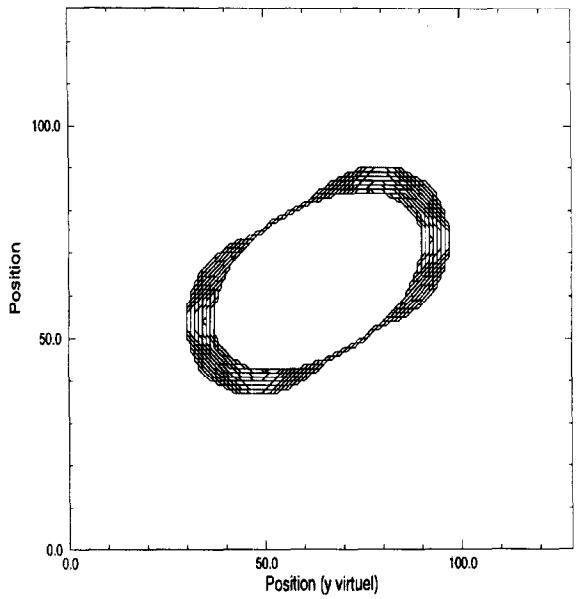

Fig. 8. Evolution of the restored function support with the number of iterations in the case of the Gaussian pattern.

4.4. Algorithms properties

4.4.1. Algorithms and regularization

The previous algorithms were introduced without taking into account any regularization condition. In the direct algorithm case, if we take into account the wavelet compactness, the wavelet inverse transform and the positivity thresholding, the regularization seems to be associated to a minimum support constraint: the number of not null pixels is similar to the number of given wavelet coefficients; it is impossible to reduce this number without loss of the consistency.

The gradient algorithm results from a least mean squares (LMS) condition. The number of pixels can be higher than the number of given wavelet coefficients, which leads to an infinity of solutions with a null distance between the given and the restored wavelet coefficients. Thus the LMS condition is not sufficient to qualify this algorithm in this specific case. Let us return to the inverse problem; we write it as

$$\mathscr{V}(r) = \sum_p \gamma(r, p)\mathscr{F}(p), \tag{59}$$

where r designs the element of $\mathscr{D}$, and p is a pixel of the image function $\mathscr{F}$. The coefficients $\gamma(r, p)$ are derived of the wavelet transform with the *à trous* algorithm. If the number of pixels is greater than the number of known wavelet coefficients, we cannot solve system (59) without a regularization condition. We consider the minimum of energy one: $\sum_p \mathscr{F}^2(p)$ is minimum. Taking into account the constraints we obtain

$$\mathscr{F}(p) - \sum_r \lambda(r)\gamma(r, p) = 0, \tag{60}$$

where $\lambda(r)$ is the Lagrange multiplier associated to $\mathscr{V}(r)$. In fact, we can also consider $\lambda(r)$ as a wavelet structure, and relation (60) means that the function is reconstructed from this wavelet structure. We can remove $\mathscr{F}(p)$; this leads to the relation

$$\mathscr{V}(r) = \sum_s \Gamma(r, s)\lambda(s), \tag{61}$$

where

$$\Gamma(r, s) = \sum_p \gamma(r, p)\gamma(s, p). \tag{62}$$

The resolution of Eq. (61) can be done iteratively, from example with Van Cittert's algorithm:

$$\lambda^{(n)}(r) = \lambda^{(n-1)}(r) + \mathscr{V}(r) - \sum_s \Gamma(r, s)\lambda^{(n-1)}(s). \tag{63}$$

Relation (63) can be rewritten taking into account Eqs. (60) and (61):

$$\lambda^{(n)}(r) = \lambda^{(n-1)}(r) + \mathscr{V}(r) - \sum_p \gamma(r, p)\mathscr{F}^{(n-1)}(p). \tag{64}$$

Now we multiply the equation by the matrix $\gamma(r, p)$ and we get

$$\mathscr{F}^{(n)}(p) = \mathscr{F}^{(n-1)}(r) + \sum_r \gamma(r, p)\left[\mathscr{V}(r) - \sum_p \gamma(r, p)\mathscr{F}^{(n-1)}(p)\right]. \tag{65}$$

Formally, relation (65) is strictly the same as the one derived from the gradient with a fix step ($\omega = 1$) and taking into account the thresholding outside the volume $\mathscr{D}$ in WTS. The gradient algorithm can be so derived from the minimum energy regularization condition.

4.4.2. Reconstruction algorithms as projection operators

We saw that different reconstruction algorithms lead to different restored images. This fact is directly connected to the ill-posed property of this inverse problem. In fact, we always get

$$\mathscr{W}(r) \approx \mathscr{V}(r) \quad \forall r \in \mathscr{D}, \tag{66}$$

where $\mathscr{W}(r)$ designs the wavelet transform of the restored image. The quality of the approximation can be limited only by the computer precision.

If we apply on the image $\mathscr{F}(p)$ this vision model, we again extract in the same $\mathscr{D}$ region the same wavelet coefficients. The same reconstruction algorithm restores the same image function $\mathscr{F}(p)$. The object reconstruction algorithm $\mathscr{P}$ can be considered as a projection operator. But $\mathscr{P}$ is not a linear operator. The non-linearity is many times introduced in this procedure: in order to define the volume $\mathscr{D}$ by the thresholding in WTS, and by the thresholding for assuming the positivity constraint.

4.4.3. Restoration of noise Gaussian patterns

We have done a set of numerical experiments with noisy Gaussian patterns. The restoration quality was always better with the gradient algorithm than with the direct one. We remarked also that the convergence with a fix step leads always to a stable solution, while the variable step algorithm leads to instabilities for a low signal to noise ratio (SNR). SNR is defined as the ratio of the standard deviation of the signal to the noise one.

In Fig. 9 we plotted the Gaussian pattern with SNR equal to 10 and its corresponding restoration using the gradient algorithm. The pattern is quite correctly restored, and the convergence is quite similar to the one without noise. In Fig. 10 SNR is equal to 1; some distortions exist but the accuracy is generally sufficient. In Fig. 11 SNR is equal to 0.1; the restoration is too bad for a further analysis.

These experiments show that it is possible to extract a significant pattern even for a small SNR. This would be quite impossible by the other vision models we described in the introduction.

4.4.4. Influence of close objects

In the upper experiments, we have considered one isolated Gaussian, but generally astronomical objects may be close, and it would be difficult to

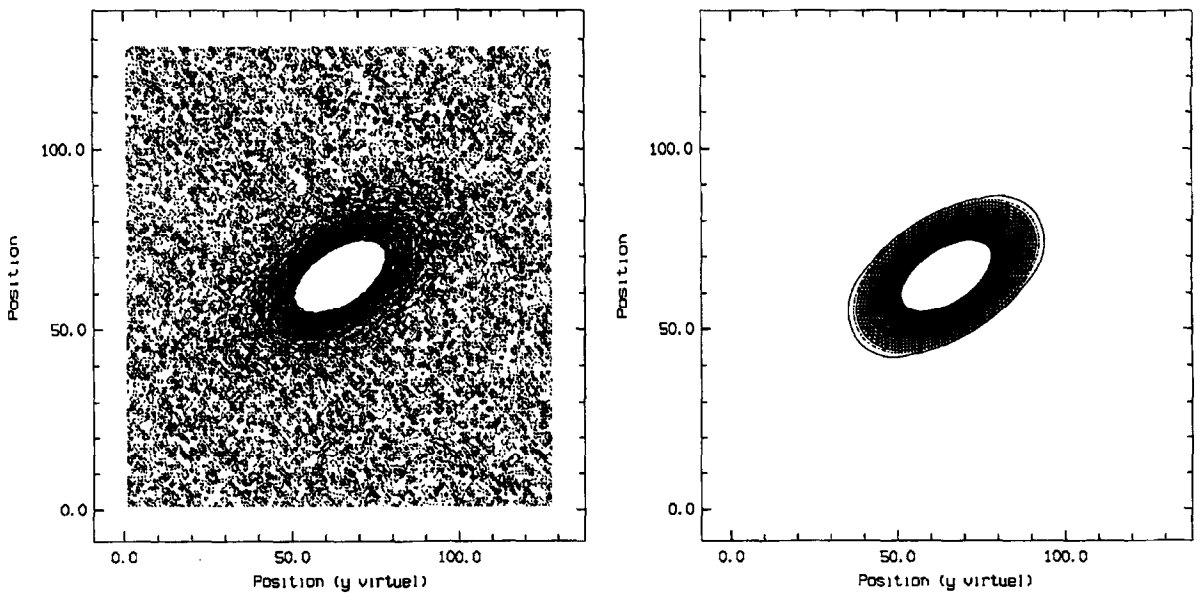

Fig. 9. Gaussian pattern with SNR 10 and its restored image by the gradient algorithm.

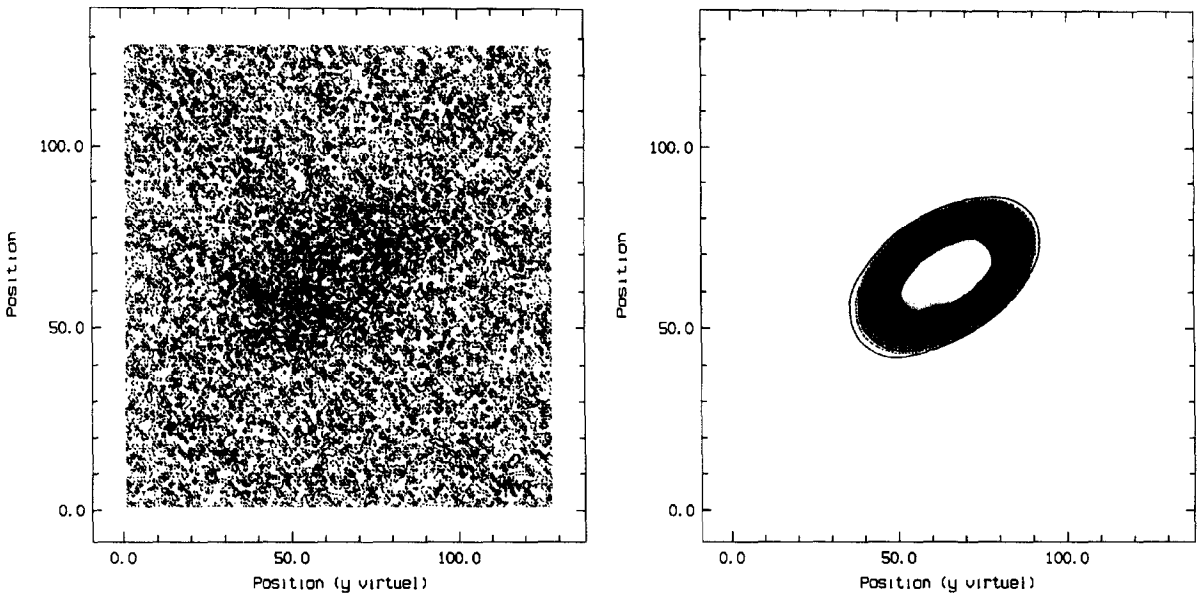

Fig. 10. Gaussian pattern with SNR 1 and its restored image by the gradient algorithm.

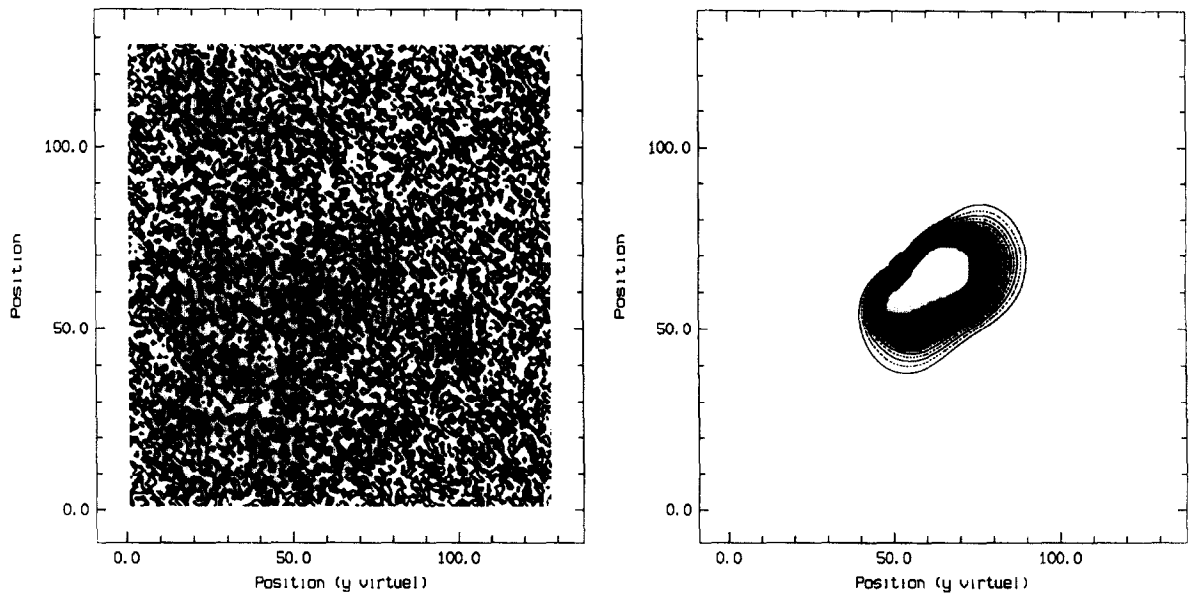

Fig. 11. Gaussian pattern with SNR 0.1 and its restored image by the gradient algorithm.

analyze them separately. We consider now two Gaussian patterns at a variable distance.

In Fig. 12 the sum of two Gaussian patterns at distance 4σ is plotted, while the restoration of the left component is plotted in Fig. 13. The algorithm needs always to work with $I_{\max+1}$ scales, but the maximum can belong to a field containing the two objects.

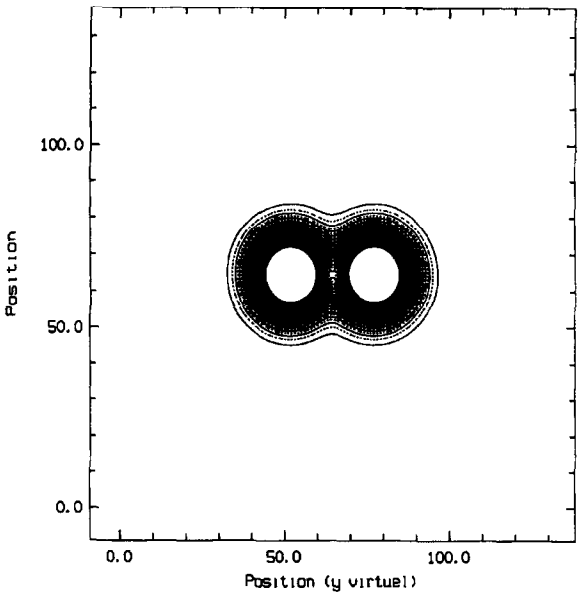

Fig. 12. The sum of the Gaussian patterns at distance 4σ.

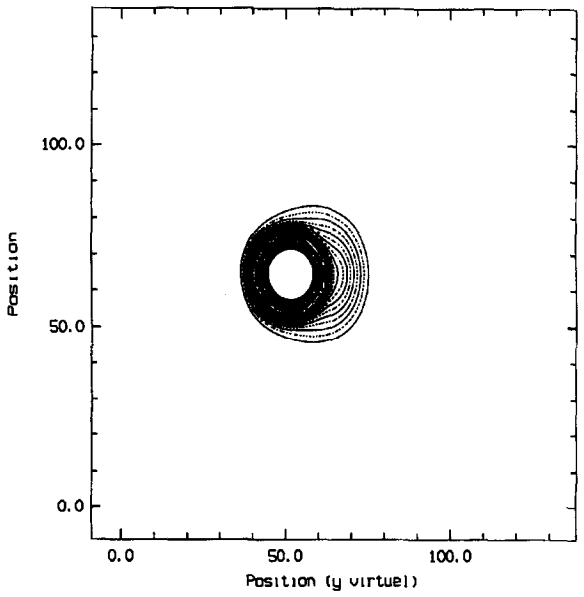

Fig. 13. The reconstruction of the left Gaussian pattern.

In the case of too close objects, the reconstruction can be improved by the following iteration. Let us consider an image $\mathscr{F}$ sum of two objects with images $\mathscr{F}_1$ and $\mathscr{F}_2$. Their wavelet transforms are

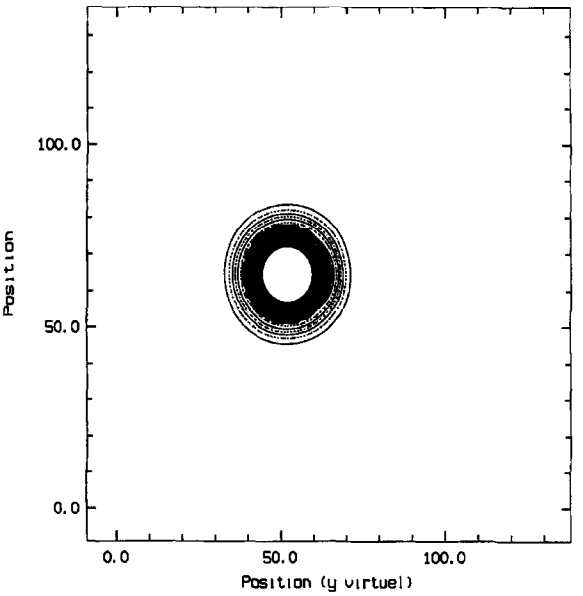

Fig. 14. The reconstruction of the left Gaussian pattern after taking into account the influence of the right component.

$\mathscr{W}_1$ and $\mathscr{W}_2$. Their significant wavelet structures are $\mathscr{V}_1$ (in $\mathscr{D}_1$) and $\mathscr{V}_2$ (in $\mathscr{D}_2$). If the objects are too close, $\mathscr{F}_2$ brings a significant contribution to $\mathscr{V}_1$, and $\mathscr{F}_1$ to $\mathscr{V}_2$:

$$\mathscr{V}_1 = \mathscr{V}_{11} + \mathscr{V}_{12}, \tag{67}$$

where $\mathscr{V}_{11}$ is the $\mathscr{W}_1$ coefficients $\in \mathscr{D}_1$ and $\mathscr{V}_{12}$ the $\mathscr{W}_2$ coefficients $\in \mathscr{D}_1$.

We improve the $\mathscr{F}_1$ restoration if we reduce the component $\mathscr{V}_{12}$, i.e. the $\mathscr{F}_2$ influence. We get an approximate solution $\tilde{\mathscr{F}}_2$ of $\mathscr{F}_2$. Subtracting $\tilde{\mathscr{F}}_2$ from the initial image $\mathscr{F}(k, l)$ the influence of $\mathscr{F}_2$ on $\mathscr{F}_1$ obviously decreases. We can do the same operation for $\mathscr{F}_1$. Then we iterate up to the convergence.

This algorithm leads to a real improvement of the quality of the restoration, for intermediate distances. For too close patterns, the initial patterns are too far from the real ones, and the algorithm does not give a correct solution. In Fig. 14 we have plotted the effect on the left Gaussian component. The quality of the restoration is quite perfect, in spite of the interaction between the patterns.

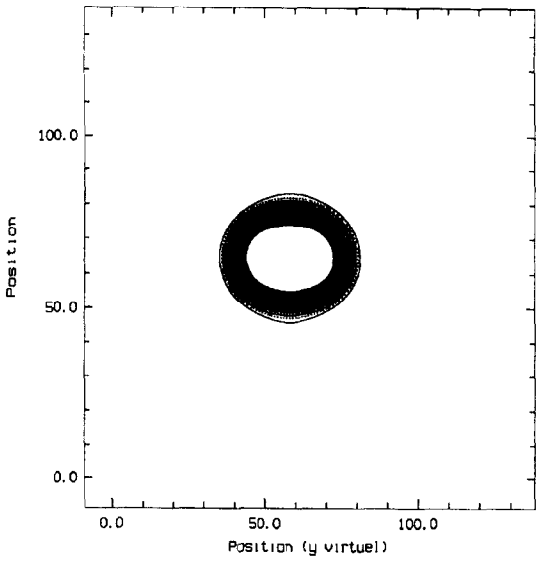

Fig. 15. The reconstruction of the sum of two Gaussian patterns at 2σ.

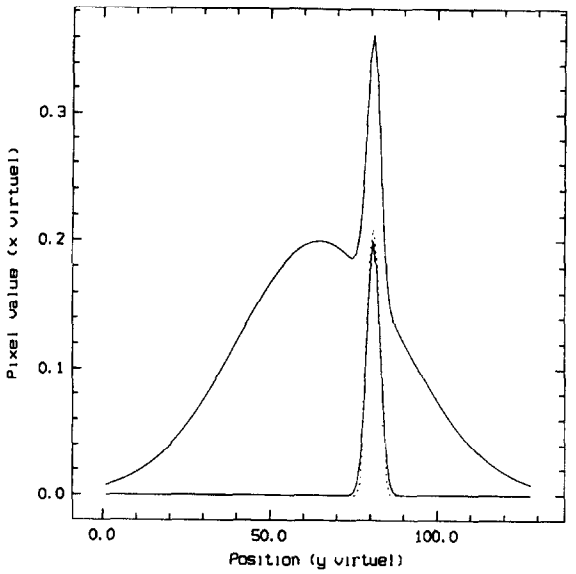

Fig. 16. The central cut of the superimposed Gaussian patterns. The original narrow pattern is plotted in solid line and the restored one in dashed line.

The algorithm could be applied to more patterns, but the complexity of the computations gives a serious restriction on the number of objects to be restored.

The algorithm restores each component if the distance d is greater than 3σ. In Fig. 15 we have plotted restoration obtained on the sum of two Gaussian patterns at a distance 2σ. We have not succeeded in separating these patterns by our vision model.

4.4.5. Superimposed patterns

At last, we examine another important case, the one of superimposed patterns. In Fig. 16 we have plotted a central cut of the image of a narrow Gaussian function superimposed on a larger one. We have plotted in the same figure the original narrow pattern and the restored one. We remark that the influence of the larger background structure is negligible.

The quality of the restoration depends on the separation between the patterns in WTS. We get no significant bias for a background pattern which can be considered as locally constant for the narrow Gaussian function.

5. Conclusion

We have built a procedure which permits to extract the whole set of objects contains in an image. The objects are defined as fuzzy structures of different sizes, hierarchically superimposed. This vision model resulting from the wavelet transform permits to detect, measure and recognize an object as complex as possible. The procedure does not introduce any prior information on the stellar profile or on the scale of the background variations. This is very important for automated procedures.

The detection takes into account the statistical noise. We have admitted a Gaussian noise, but this can be extended to other kinds of noise, taking into account the resulting distribution of the wavelet coefficients. Some experiments on real astronomical images have shown that the detection is performed up to the faintest objects we can observe.

The object characteristics are simply computed from the image which is restored from each of them. Our experiments showed also that the accuracy for the photometry is compatible with the noise

statistic. In another paper for an astronomical review we will examine with details the performances of the vision model, compared to previous ones.

The main disadvantage lies in the number of used data. The *à trous* algorithm increases the data by the number of scales. In our experiments we used 4–5 scales. The increase is too high for large astronomical images. The introduction of a less redundant algorithm would lead to accelerate the extraction of the information and to a data compression. The adaptation to an isotropic pyramidal transform [3] leads to some difficulties related to the interscale connection.

Acknowledgements

We thank A. Lannes, J.M. Petit and J.L. Starck for helpful discussions and comments.

References

[1] F.J. Anscombe, "The transformation of Poisson, binomial and negative-binomial data", *Biometrika*, Vol. 15, 1948, pp. 246–254.

[2] A. Bijaoui, "Skybackground estimation and applications", *Astron. Astrophys.*, Vol. 84, 1980, pp. 81–84.

[3] A. Bijaoui, "Algorithmes de la transformation en ondelettes. Applications en astronomie", in: *Ondelettes et Paquet d'Ondes*, INRIA, 1991, pp. 115–140.

[4] A. Bijaoui, G. Lago, J. Marchal and C. Ounnas, "Le traitement automatique des images en Astronomie", in: *Traitement des Images et Reconnaissance des Formes*, INRIA, 1978, pp. 848–854.

[5] R.M. Bracewell, *The Fourier Transform and its Applications*, McGraw-Hill, New York, 1965, Chapter 10, p. 189.

[6] I. Daubechies, "Orthonormal wavelets of finite support – Connection with discrete filters", in: J.M. Combes et al., eds., *Wavelets*, Springer, Berlin, 1989, pp. 38–66.

[7] G. Demoment, "Image reconstruction and restoration: Overview of common estimation structures and problems", *IEEE Trans. Acoust. Speech Signal Process.*, Vol. 37, 1989, pp. 2024–2036.

[8] B.R. Frieden, "Image enhancement and restoration", in: T.S. Huang, ed., *Picture Processing and Digital Filtering*, Springer, Berlin, 1975, pp. 177–249.

[9] A. Grossmann, R. Kronland-Martinet and J. Morlet, "Reading and understanding continuous wavelet transform", in: J.M. Combes et al., eds., *Wavelets*, Springer, Berlin, 1989, pp. 2–20.

[10] W.W. Harman, *Principles of the Statistical Theory of Communication*, McGraw-Hill, New York, 1963, Chapter 11, p. 217.

[11] M. Holdschneider, R. Kronland-Martinet, J. Morlet and P. Tchamitchian, "A real-time algorithm for signal analysis with the help of the wavelet transform", in: J.M. Combes et al., eds., *Wavelets*, Springer, Berlin, 1989, pp. 286–297.

[12] L. Landweber, "An iteration formula for Fredholm integral equations of the first kind", *Amer. J. Math.*, Vol. 73, 1951, pp. 615–624.

[13] O. Le Fèvre, A. Bijaoui, G. Mathez, J.P. Picat and G. Lelièvre, "Eletronographic BV photometry of three distant cluster of galaxies. I. Method", *Astron. Astrophys.*, Vol. 154, 1986, pp. 92–96.

[14] J. Littlewood and R. Paley, "Theorems on Fourier series and power series", *J. London Math. Soc.*, Vol. 6, 1931, pp. 230–233.

[15] S. Mallat, "Multifrequency channel decompositions of images and wavelet models", *IEEE Trans. Acoust. Speech Signal Process.*, Vol. 37, 1989, pp. 2091–2110.

[16] J. Morlet, G. Arens, E. Fourgeau and D. Giard, "Wave propagation and sampling theory I and II", *Geophysics*, Vol. 47, 1982, pp. 203–236.

[17] R. Murenzi, "Wavelet transforms associated to the *n*-dimensional Euclidean group with dilations: Signal in more than one dimension", in: J.M. Combes et al., eds., *Wavelets*, Springer, Berlin, 1989, pp. 239–246.

[18] F. Murtagh, J.L. Starck and A. Bijaoui, "Image restoration with noise suppression using a multiresolution support", *Astron. Astrophys. Sup. Ser.*, Vol. 112, 1995, pp. 179–189.

[19] W. Pratt, *Digital Image Processing*, Wiley, New York, 1978, Chapter 8, p. 207.

[20] A. Rosenfeld, *Picture Processing*, Academic Press, New York, 1969, p. 127.

[21] E. Slezak, A. Bijaoui and G. Mars, *Astron. Astrophys.*, Vol. 200, 1988, p. 1–20.

[22] E. Slezak, G. Mars, A. Bijaoui, C. Balkowski and P. Fontanelli, *Astron. Astrophys. Sup. Ser.*, Vol. 74, 1988, pp. 83–106.

[23] J.-L. Starck and A. Bijaoui, "Filtering and deconvolution by the wavelet transform", *Signal Processing*, Vol. 35, No. 3, February 1994, pp. 195–211.

[24] R.S. Stobie, "The Cosmos image analyzer", *Pattren Recognition Lett.*, Vol. 4, 1986, pp. 317–324.

[25] G. Strang, "Wavelets and dilation equations: A brief introduction", *SIAM Rev.*, Vol. 31, 1989, pp. 614–627.

[26] M. Unser and A. Aldroubi, "Polynomial splines and wavelets – A signal processing perspective", in: C.K. Chui, ed., *Wavelets, A Tutorial in Theory and Applications*, Academic Press, New York, 1992, pp. 91–122.

[27] P.H. Van Cittert, *Z. Physik*, Vol. 69, 1931, p. 298.